PAPER

Check for updates

Preparation of acid-driven magnetically imprinted micromotors and selective loading of phycocyanin†

Guangdong Yang,‡[a] Jiajing Liu,‡[c] Zhong Zhang, ✱[ab] Li Yuan, [a] Hongye Tian [a] and Xingbin Yang [a]

Phycocyanin, a macromolecular protein known for its robust fluorescence, proves to be highly suitable for verifying the successful deposition of imprinted layers. In this study, an acid-propelled magnetic micromotor was successfully fabricated by utilizing surface imprinting and self-propelled nanomotor technology to achieve selective loading and capture of targets such as phycocyanin for future applications in environmental monitoring and precision drug delivery *in vivo*. This micromotor features a distinct recognition layer achieved through a template electrodeposition method. The outermost imprint layer of the micromotor was meticulously crafted using poly(3,4-ethylenedioxythiophene)/poly(sodium-4-styrenesulfonate) in the presence of a template, while the Pt layer serves as the supportive foundation, the Ni layer acts as the magnetic guidance component, and the innermost layer consists of metal Zn. In acidic environments, the Zn reacts to generate bubbles, which propels the micromotor's motion. The micromotor was comprehensively characterized using techniques such as scanning electron microscopy. Findings highlight the exceptional self-propulsion of the Zn-based micromotor, which is a fusion of molecular imprinting and micromotor technologies. This innovative design achieves an impressive maximum velocity of approximately 100 $\mu m\ s^{-1}$, as well as commendable magnetic steering performance. Furthermore, the micromotor demonstrates the ability to imprint target protein through the imprint layer, enabling selective recognition and capture for transport of specific phycocyanin. *In vitro* cytotoxicity tests have also demonstrated that the micromotors are non-toxic to cells. This breakthrough concept offers a novel avenue for realizing targeted capture and transport of specific nutrients within the human gastric environment.

1. Introduction

In recent years, the rapid development of self-driven micro and nanomotor technology has achieved significant advancements in various applications, such as environmental remediation,[1] drug delivery,[2] water purification,[3] DeoxyriboNucleic acid (DNA) recognition,[4] and other fields. This trend represents a crucial direction within the current domain of nanoscience. Self-driven micro and nanomotors, as implied by their name, are characterized primarily by their small size, operating at the micro and nanoscale levels, and displaying spontaneous movement. These motors can convert different forms of energy, such as chemical, electric, and light energies, into kinetic energy.

Categorized by their driving mechanisms, micromotors generally fall into five distinct categories: chemical-, magnetic-, optical-,[5–7] ultrasonic-, and electric field-driven.[8] Particularly, chemical-driven micromotors, which convert chemical energy into kinetic energy, are widely used and possess significant potential. Depending on the specific fuels utilized, they can be classified into hydrogen peroxide,[9,10] water,[11,12] hydrazine,[13] and acid-driven[14] types.

The exploration of micromotors originated from a captivating chemical experiment. Whitesides *et al.* (2002)[15] successfully designed and developed a self-propelled device using hydrogen peroxide as fuel, catalyzed by Pt to produce bubbles.

[a] *Shaanxi Engineering Laboratory for Food Green Processing and Safety Control, Engineering Research Center of High Value Utilization of Western Fruit Resources, Ministry of Education, College of Food Engineering and Nutritional Science, Shaanxi Normal University, Xi'an, Shaanxi, 710119, P. R. China. E-mail: zzhang@snnu.edu.cn; Fax: +86 10-85310517; Tel: +86 10-85310517*

[b] *Xi'an Key Laboratory of Characteristic Fruit Storage and Preservation, Shaanxi Key Laboratory for Hazard Factors Assessment in Processing and Storage of Agricultural Products, Shaanxi Normal University, Xi'an, Shaanxi, 710119, P. R. China*

[c] *School of Food Science and Engineering, South China University of Technology, Guangzhou, Guangdong, 510641, P. R. China*

† Electronic supplementary information (ESI) available. See DOI: https://doi.org/10.1039/d3tb02021e

‡ Contributed equally to this work.

10728 | *J. Mater. Chem. B*, 2023, **11**, 10728–10737

This journal is © The Royal Society of Chemistry 2023

This experiment garnered considerable attention, prompting researchers to delve into the study of self-driven micro and nanoscale devices, marking the inception of micromotor research. The year 2004 witnessed the development of the first Au/Pt catalytic micromotor,[16] ushering in a period of rapid nanomotor evolution. As micromotor technology progressed, various preparation methods emerged, including template-assisted electrodeposition,[17] physical vapor deposition,[12] crimping method,[18] and Pickering emulsion method.[9,19] Each method boasts unique features, enabling the synthesis of diverse micromotor shapes, such as tubes, rods, spirals, and spheres. Researchers continuously strive for excellence, setting high standards for motion performance and aspiring to attain precise and controllable micromotor manipulation. Techniques such as magnetic,[20] ultrasonic,[21] and electric fields[22] have been developed to regulate micromotor movement.

Despite the rapid diversification of micromotor types, the technology system remains incomplete. At present, most micromotors employ hydrogen peroxide as fuel and Pt or catalase as catalysts for motion. However, the costliness of Pt as a precious metal hampers its large-scale application. Although enzymes exhibit favorable biocompatibility, they are susceptible to inactivation and adverse reaction conditions, posing challenges to practical micromotor deployment. Consequently, the replacement of fuel and the exploration of cost-effective, biocompatible, and easily controllable micromotor alternatives have become urgent priorities.

Molecular imprinting technology often described as a technique for creating molecular locks to match molecular keys, involves the formation of molecularly imprinted polymers (MIPs) featuring tailored binding sites that complement template molecules in shape, size, and functional groups.[23] This technology's specific recognition properties hold promising applications in substance-specific adsorption, separation, and loading. Among various synthesis methods for MIPs, bulk imprinting, surface imprinting, epitope imprinting, and solid-phase synthesis surface imprinting stands out by grafting MIPs onto substrate surfaces. This method boasts thin imprinting layers, easy template removal, rapid mass transfer, customizable shapes, and the introduction of smart materials. Consequently, the fusion of surface imprinting and micromotor technology has yielded substantial advancements, enhancing micromotor effectiveness in detection and transportation. Gao *et al.*[24] utilized electrodeposition to create antibiotic-imprinted micromotors using fluorescein isothiocyanate-labeled avidin as a template, enabling protein capture and transportation. Phycocyanin (PC), is an oligomeric protein consisting of the α and β subunit polypeptides and an open-chain tetrapyrrole structured chromophore cofactor, emitting fluorescence around 615–640 nm with high stability and sensitivity, has emerged as an appealing fluorescent marker with diverse applications, particularly in life sciences, biomedicine, and environmental studies.[25,26] By leveraging phycocyanin's robust red fluorescence signal at 620 nm, this study selected selective capture, loading, and fluorescence detection of phycocyanin in water samples as a visual characterization method. Zhang's team[27] successfully adsorbed

phycocyanin with casein-porous starch microgels, achieving *in vivo* fluorescence imaging with zebrafish. In addition, Zhang's team[28] employed phycocyanin's fluorescence attributes to prepare a label-free fluorescent western blot micromotor *via* electrodeposition, enabling qualitative and quantitative phycocyanin detection and preliminary seawater analysis.

The above approach highlights the micromotor's enhanced recognition ability through MIP, significantly enhancing reaction sensitivity—a pivotal contribution in material transportation and rapid detection. However, few reports have explored the fusion of the two technologies. Consequently, continued exploration and development of their amalgamation are vital for producing micromotors with diverse functional characteristics, maximizing their benefits across a range of applications.

This study addresses the aforementioned challenges by combining micromotor self-propulsion technology with molecular imprinting technology. The transition from hydrogen peroxide to acid as the fuel source and the use of poly (3,4-ethylenedioxythiophene)/poly(sodium-4-styrenesulfonate) (PEDOT/PSS)—a substance with strong selective protein binding properties—as the imprinting layer enabled the creation of a Zn-based acid-driven magnetic imprinting micromotor *via* template electrodeposition. This micromotor possesses distinct recognition capabilities and superior loading performance, facilitating the capture and loading of phycocyanin in complex water samples. The study underscores the feasibility of uniting imprinting technology and micromotor driving technology to achieve material capture, transportation, separation, and removal. Notably, the micromotor exhibits high selectivity for phycocyanin capture, efficient load visualization, simple production, low cost, short preparation time, excellent biocompatibility, and suitability for acidic environments. Furthermore, the Zn involved in the reaction serves as an essential trace element supplement for the human body, promoting harmlessness and beneficial effects. In the future, *in vivo* delivery within the human stomach environment holds exciting potential.

2. Experimental section

2.1 Reagents and materials

Phycocyanin was kindly provided by Shandong Oriental Ocean Company (Yantai, China) and used as the template protein. Bovine serum albumin (BSA), casein, β-lactoglobulin, and DAPI were purchased from Aladdin (Shanghai, China). 3,4-Ethylenedioxythiophene (EDOT), PSS ($M_w \sim 70\,000$), and chloroplatinic acid ($H_{14}Cl_6O_6Pt$) were purchased from Aladdin (Shanghai, China). Lead nitrate ($Pb(NO_3)_2$) was purchased from Sigma (USA). Nickel amino sulfonate (Ni ($NH_2SO_3)_2 \cdot 4H_2O$) was purchased from Sinopharm Group Chemical Reagent Co., Ltd. Nickel dichloride ($NiCl_2$) was purchased from Tianjin Kemio Chemical Reagent Co., Ltd (Shanghai, China). Hydrochloric acid (HCl), absolute ethyl alcohol (C_2H_5OH), boronic acid (H_3BO_3), sulphuric acid (H_2SO_4), CCK-8 reagent, and white vitriol ($ZnSO_4$) were purchased from Tianjin Kemio Chemical Reagent Co., Ltd. Carrene (CH_2Cl_2) was purchased from Tianjin Fuyu Fine Chemical

Co., Ltd. (Shanghai, China). Triton X-100 ($C_{16}H_{26}O_2$) was pursed from Xilong Science Co., Ltd. All solvents and chemicals were of analytical grade and used directly without further purification, unless otherwise specified. Doubly purified deionized (18.2 MΩ, Millipore, MA, USA) was used for the preparation of all aqueous solutions.

2.2 Experimental method

2.2.1 Treatment of polycarbonate membrane. The two sides of the experimental polycarbonate film are different, divided into frosted surface and, we only spray with Au on the frosted surface. The frosted surface of polycarbonate film with diameter of 25 mm and pore size of 2 μm was initially sprayed with Au (200 s) at room temperature by ion sputtering instrument for conduction (SCD005). The smooth surface for electrodeposition is not treated. The resistance of non-sprayed and sprayed films was measured by a current meter to determine whether the conductivity of the template was good during electrodeposition. Then, the air inside its pore diameter was removed by ultrasonic vibration for 3 min, and it was placed in 0.5 mg mL^{-1} of phycocyanin solution, soaked for 20 min, and left to dry in air for 20 min. Finally, it was washed with pure water for 2–3 times and dried until use.

2.2.2 Preparation of PEDOT/PSS–Pt–Ni–Zn micromotors. The electrochemical cell used was specially customized and assembled using polytetrafluoroethylene material. The photos of the assembled electrochemical cell and the details of various electrodes are shown in Fig. S1 (ESI†). The prepared cell could hold about 8 mL of the solutions, and the polycarbonate film after the above treatment was placed on the aluminum foil as a working electrode. The Au-sprayed side was connected to the aluminum foil, and the non-Au-sprayed side was facing up. Pt wire was used as the counter electrode, and Ag/AgCl (saturated potassium chloride) was used as the reference electrode. Electrochemical deposition begins after assembly. The configuration of the deposition solution used in the electrochemical deposition process can be found in the ESI.†

Tubular micromotors were prepared by template electrochemical deposition method following four steps. Briefly, PEDOT layers were initially deposited potentiostatically at +0.80 V using a charge of 4C from a plating solution containing 10 mM EDOT and 125 mM PSS. Subsequently, an initial Pt layer was deposited galvanostatically at −2 mA for 400 s from a Pt plating solution to improve the mechanical properties of the polymeric layer. Then, an intermediate Ni layer was deposited potentiostatically at −1.3 V for 3.0C from a Ni plating solution to provide magnetic guidance. Finally, the inner catalytic Zn was deposited potentiostatically at −1.3 V for 10.0C to provide driving power. The relevant methods and parameters of electrodeposition are detailed in Table S1 (ESI†).

The electrodeposited polycarbonate film was washed 2–3 times with water, and its front and back sides were manually polished with 0.05 μm alumina paste to remove the Au sprayed on the film's matte surface, as well as the sediment on the smooth surface. Then, the polished polycarbonate membrane was shaken and dissolved with dichloromethane for 30 min.

In this manner, PEDOT/PSS–Pt–Ni–Zn micromotors (micromotors for short) could be separated from the membrane, and the bound protein template could be separated from the micromotors, and then washed twice with dichloromethane. The dispersed micromotors were collected by centrifugation at 8000 rpm for 3 min, and finally washed 3 times with absolute ethanol. The micromotors were stored in absolute ethanol at room temperature, and the micromotors were washed 2–3 times with water before use.

The preparation of non-imprinted micromotors (NIPs) was similar to the procedure described above, except that the step of soaking the membrane in phycocyanin solution was omitted during the treatment of the polycarbonate membrane.

2.2.3 Morphological characterization. The micromotor solution was sonicated to disperse evenly. Preliminary observation of micromotor morphology was performed using a digital microscope (CKX53). The micromotor solution was dropped on the slide, the magnification of the microscope objective was adjusted to 10×, and the target object was found under the microscope for preliminary observation to determine whether the micromotor was synthesized successfully. The magnification of the objective was adjusted to 40×, and the morphology was observed to verify whether the micromotor was tubular structure. Then, the feasibility of the template electrodeposition method was verified.

2.2.4 Scanning electron microscopy (SEM) and energy dispersive analysis (EDA) characterization. The micromotor solution was sonicated to disperse evenly. The micromotor solution was absorbed on the clean silicon wafer and placed it in a 45 °C hot air drying oven to dry. SEM (Quanta 200) was used to observe the morphology of micromotors on silicon wafers, and EDA was used to analyze the component elements to verify whether the required elements were successfully deposited.

2.2.5 Magnetic property determination. The magnetic rod was used to adsorb the micromotor stored in the centrifuge tube, and whether it moved in the direction of the magnetic rod was observed. If the motor moves with the magnet bar, then the micromotor is magnetic and the metal Ni is successfully deposited inside. If it does not follow, then it is weak-magnetic or non-magnetic; that is, the amount of metal Ni deposition is less or there exists no deposition at all, and the preparation of the micromotor has failed. Subsequently, the micromotors were positioned under the 10× objective of an optical microscope (CKX53), and the effect of the change in the direction of the magnetic field on the micromotors was observed.

2.2.6 Drive determination and condition investigation. HCl solution (with Triton-X100 as surfactant) was dropped into the micromotor solution on the slide, and the bubbles were observed under an optical microscope (CKX53) with a 10× objective lens to detect whether the Zn electrodeposition was successful.

In addition, although the micromotor solution is initially stored in absolute ethanol, the mixture of absolute ethanol and HCl will result in a loss of clarity in the solution, potentially

10730 | *J. Mater. Chem. B*, 2023, **11**, 10728–10737

This journal is © The Royal Society of Chemistry 2023

affecting the observation results. Therefore, the micromotor needs to be cleaned with water initially, such that it is dispersed in the aqueous solution, and the observation can then be performed. However, the surface tension of water is relatively large, and the internal aperture of the micromotor is extremely small. The situation where the solution possibly struggles to penetrate the pore to react might necessitate the addition of surfactant to improve this situation. By fixing the pH value and taking the surfactant content as a variable, the effect of surfactant on the bubble generation of the micromotor was investigated, and the optimal parameters were selected.

2.2.7 Fluorescence measurement of phycocyanin. Phycocyanin solution (0.5 mg mL^{-1}) was prepared, and phycocyanin solution (0.2 mL) was then added to 0.2 mL of micromotor solution that had been fully ultrasonic and evenly shaken. After soaking for 20 min, the supernatant was removed, 0.1 mL of ultrapure water was added, and the micromotor solution was treated with a vortex oscillator to make it evenly dispersed. To determine whether the imprinted micromotors recognized the bound phycocyanin, a laser confocal microscope (FV1200) was used to observe the fluorescence state of the micromotor at 0 min and 20 min at 633 nm excitation wavelength using NIP as a control.

2.2.8 Determination of selective adsorption capacity of imprinting layer. Concentrations of 0, 0.1, 0.2, 0.3, 0.4, 0.5 mg mL^{-1} of phycocyanin solution, bovine serum albumin (BSA) solution, casein solution, and β-lactoglobulin solution were prepared to make a standard curve. Thereafter, the micromotor solution was ultrasonically mixed and equally divided into four centrifuge tubes. The supernatant was removed after centrifugation, and 1 mL of phycocyanin, BSA, casein, and β-lactoglobulin solution was added at a concentration of 0.3 mg mL^{-1}. The supernatant liquid was taken after centrifugation, and the change in protein concentration before

and after adsorption was measured to determine the selectivity of the imprinted layer.

To determine the protein concentration, the absorbance values of phycocyanin, casein, and β-lactoglobulin solutions were determined by the Folin-reagent method at 450 nm, and the absorbance value of the BSA solution was determined at 562 nm.

2.2.9 Cytotoxicity testing of micromotors. Human liver cells were selected for cytotoxicity test by Cell Counting Kit-8 (CCK-8). In the 96-well plate, 100 μL of cell suspension and culture medium were added respectively, mixed well and incubated in the incubator for 12 h, 10 μL of PBS was added to the blank control group, and 10 μL of imprinted micromotor solution with the concentration of 0, 1, 0.1, 0.01, 10^{-3} mg mL^{-1} ultrasonically dispersed for 3 min, was added to the positive group, and incubated in the incubator for 12 h. After that, 10 μL of CCK-8 reagent was added for 4 h. After the reaction, the absorbance value at 450 nm was measured for the cell viability.

2.2.10 Application of micromotors in complex environments. The study examined the fluorescence effect of phycocyanin-conjugated micromotors in complex cellular environment to broaden the application ability of micromotors in actual environments. Human liver cells were cultured, resuscitated, and allowed to grow in an incubator at 37 °C. The process of passage was initiated when the cell density in the culture dish reached about 80–90%. In this process, the original medium was poured out, an appropriate proportion of trypsin was added for a digestion period of 3 min, and the medium was then added to terminate the digestion. The cells on the wall of the culture dish were repeatedly washed using a pipetting gun, ensuring their suspension. The liquid in the Petri dish was then centrifuged at 2000 rpm for 5 min, the supernatant was removed, and 1–2 mL of the medium was added and mixed evenly. Finally, a cell slide was made and placed in a 12-well plate. A small amount of cell suspension was
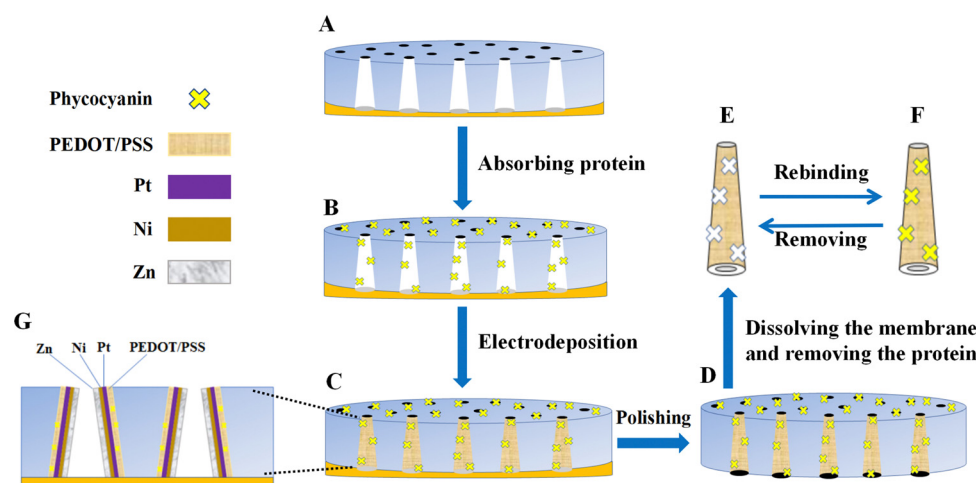

Fig. 1 Preparation principles of PEDOT/PSS–Pt–Ni–Zn imprinted micromotor: (A) polycarbonate film sprayed with Au; (B) polycarbonate membranes adsorbed with phycocyanin; (C) PEDOT/PSS imprinted layer, Pt layer, Ni layer, and Zn layer were deposited successively; (D) manual polishing of the deposited polycarbonate film to remove the Au sprayed on the bottom; (E) dissolving the membrane with dichloromethane and removing the protein to obtain the dispersed micromotors; (F) the micromotor was immersed in the phycocyanin solution, and its imprinted site recombined with phycocyanin; (G) section of the polycarbonate film after deposition.

sucked on the slide, and an appropriate amount of medium was added to the well.

The cultured cell slides were removed, 20 μL of phycocyanin adsorbed micromotor solution was dropped, and 1 drop of DAPI staining was added to stain the cells. Then, the cells were observed under a laser confocal microscope at 20× to observe whether the micromotor still had fluorescence in the cellular environment. If so, then the micromotors can be applied not only in aqueous solutions but also maintain good properties in complex cellular environments, which lays a foundation for future *in vivo* experiments.

3. Results and discussion

3.1 Preparation of PEDOT/PSS–Pt–Ni–Zn imprinted micromotors

Micromotors were prepared by template electrodeposition, and the preparation principle is shown in Fig. 1. The polycarbonate film was initially sprayed with Au for 200 s, and its resistance was measured between 4 Ω and 15 Ω using a current meter. Meanwhile, the resistance of the non-sprayed polycarbonate film was measured to be infinite, indicating that the Au-sprayed film has electrical conductivity and can be used for electrodeposition. Fig. 2(A) and (C) show the polycarbonate films used for electrodeposition and the polycarbonate films sprayed with Au, respectively. At the same time, the contact angle of water droplets in contact with the substrate was recorded. As shown in Fig. 2(B) and (D), the contact angle of the non-sprayed polycarbonate film is 72.8°, indicating a certain degree of hydrophilicity. After spraying Au on the polycarbonate film, the Au nanoparticles become non-hydrophilic, resulting in a slight decrease in the hydrophilicity of the polycarbonate film.

The contact angle increases to 82.4°. The entire synthesis of micromotors is represented in Fig. 2(E)–(H).

The outermost layer of the micromotor synthesized according to the steps is the western blot layer, and its components are PEDOT/PSS. PEDOT is a polymer conductive material with good chemical and electrochemical stability, which is often used in electropolymerization. By doping a suitable proportion of PSS, the performance of PEDOT is further improved. In this manner, the complex has excellent film formation and stability, which is highly suitable for the blotting of protein targets. The main reason is that the PEDOT/PSS complex has a strong binding ability to proteins, which can produce necessary hydrogen bonds, electrostatic interactions, and π–π interactions with proteins.[29,30] Therefore, PEDOT/PSS was selected as a protein imprinting layer. After the imprinting layer, the metal layers are Pt, Ni, and Zn, in which Pt was used as the skeleton of the micromotor, such that the micromotor has good mechanical properties. The electrodeposited solution can be found in Fig. S2 (ESI†). Ni makes the micromotor magnetic, such that its movement direction can be controlled by magnetism. Zn reacts under acidic conditions to produce bubbles that push the micromotor to move, making the micromotor motile.

3.2 Morphology of micromotors

The morphology of micromotors with Pt deposition time of 200 s was observed under a microscope with 10× (Fig. S3(A), ESI†) and 40× (Fig. S3(B), ESI†) objective magnification. In the case of 10× objective magnification, the micromotors are dispersed well after ultrasonic vibration, and most of them are in a separate state. Given the small magnification and wide field of view, the micromotors are mostly short, black, and rod-like, but the micromotors may be broken and agglomerated
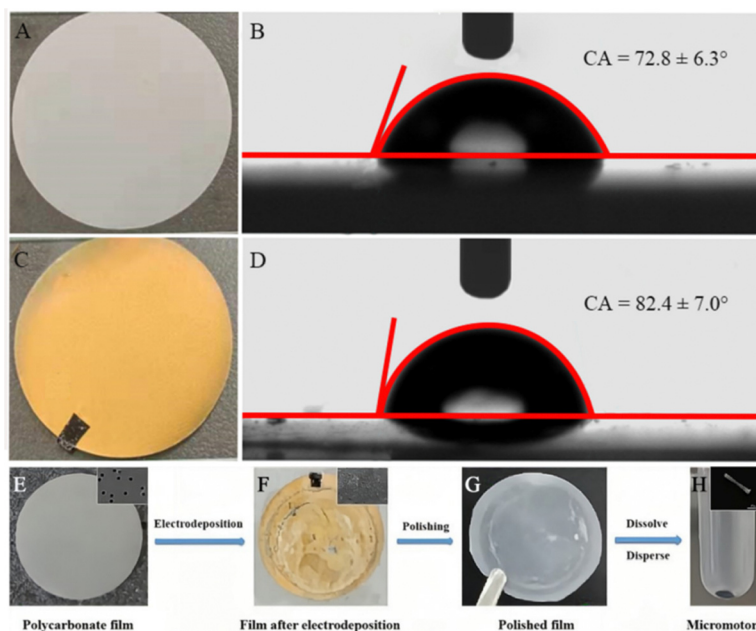

Fig. 2   (A) Photo of polycarbonate film for electrodeposition without Au spraying and (B) water contact angles on polycarbonate film. (C) Photo of Au-sprayed polycarbonate film. (D) Water contact angles on Au-sprayed polycarbonate film. (E)–(H) Further treatment of the film after electrodeposition.

10732 | *J. Mater. Chem. B*, 2023, **11**, 10728–10737

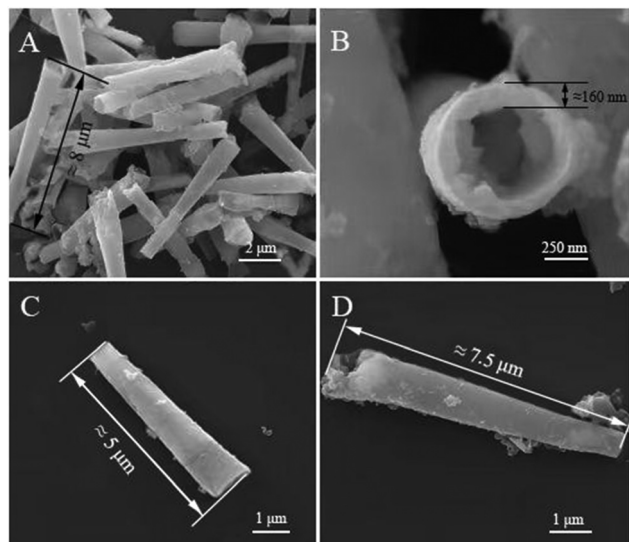This journal is © The Royal Society of Chemistry 2023

Fig. 3 SEM images of micromotor: (A)–(C) NIPs; (D) imprinted micromotor.

due to the small amount of Pt deposition and the influence of subsequent incomplete polishing of polycarbonate film. Therefore, after the deposition amount of Pt layer was adjusted to 400 s to strengthen the skeleton of the micromotor, the morphology of the micromotor was observed under the $10\times$ objective lens with an optical microscope after the ultrasonic oscillation and dispersion is uniform, as shown in Fig. S3(C) (ESI†). The fracture situation is greatly improved.

SEM was used to further observe the morphology of the prepared micromotor. As shown in Fig. 3(A) and (B), the micromotor has a conical tubular structure, the outer diameter of the two ends of the tube is about 0.7 μm and 1.1 μm, and the thickness of the tube is about 160 nm. The length of the micromotors is not uniform, generally between 5–10 μm. This result can be attributed to the thickness of the polycarbonate film being affected and decreased during the polishing process, and the micromotors may break during the centrifugation process, leading to the reduction of the length. In addition, as shown in Fig. 3(C) and (D), the surface of the NIP is relatively smooth, whereas the surface of the imprinted micromotor is extremely rough. The reason is that the imprinted micromotor is immersed in phycocyanin solution before electrodeposition, and many protein-binding sites are formed on the surface of the imprinted micromotor. In comparison with the NIP, the binding ability and sensitivity to phycocyanin will be higher, which is beneficial to the recognition and capture of phycocyanin.

3.3 Composition of micromotors

The SEM analysis shows that the appearance morphology of the micromotor basically achieves the expected effect. To obtain direct evidence to further prove that the materials and elements in the electrodeposition of the template are successfully deposited and the micromotor is constructed, EDA was used to analyze the micromotor. The results are shown in Fig. S4 (ESI†). Particularly, Zn and Ni each have two spectral peaks in the

energy spectrum diagram, which is mainly determined by the number of electron layers of the element. The more electron layers in the outer core of the element is, the more electronic transitions will occur, the more types of X-rays will be released, and the more spectral peaks will be finally reflected in the diagram. In addition, the spectrum peak of C in the figure is extremely low, but its content ranks the second among all the contents. Conversely, the spectrum peak of Zn is considerably higher than that of other elements, but its content is only slightly higher than that of C element. The reason is that the level of the spectrum peak represents the strength of the collected signal. Moreover, the energy released by the outer electron transition of different elements is also different, so the collected signal is also different. Therefore, no direct relationship exists between the number and level of spectral peaks of elements and their content.

After software correction, the weight ratio and content ratio of each element were obtained. Particularly, C (27.07%) and O (18.16%) were mainly derived from the deposition of PEDOT/PSS in the outer western blot layer of the micromotor. Pt (1.04%), Ni (6.64%), and Zn (28.02%) were mainly derived from the deposition of metal elements in their corresponding electroplating solutions. Si (16.60%) and Au (2.47%) were the substrate elements. The reason for the appearance of Si is that the liquid micromotor solution was dried on the silicon wafer before electron microscopy, and the sample was pretreated. The reason for the appearance of Au is that the sample was sprayed with Au during electron microscopy. Therefore, the required substances and elements are successfully deposited and form the micromotor, and the amount of their content mainly depends on the length of the electrodeposition time or the amount of charge. In addition, the high Zn content deposited inside the micromotor ensures that it can react in an acidic environment, producing bubbles and then moving.

3.4 Magnetic property of micromotors

The micromotor in the centrifuge tube is initially adsorbed with a magnetic stick, as shown in Video S1 (ESI†). When the magnetic force bar is at different positions, the micromotor in the centrifuge tube will move along the direction of the magnetic force bar, which proves that the magnetic metal Ni is successfully deposited in the micromotor, and the artificial navigation system for the micromotor is constructed. Subsequently, 2 μL of the prepared micromotor liquid was dropped on the slide after ultrasonic oscillation. Under the optical microscope with $20\times$ objective fold, the magnetic end of the micromotor in the ethanol liquid is attracted by the external magnetic field and shows controllable steering, as shown in Fig. 4(A)–(D). When the micromotor moves in an acidic environment, an external magnetic field can be applied to control its movement direction. In this manner, it can reach the intended position efficiently and accurately, and provide an accurate movement route for future *in vivo* delivery. See Video S2 (ESI†) for the video of magnetic guidance steering.

3.5 Motion performance of micromotors

3.5.1 Effect of surfactant on micromotor bubbles. For fixed pH = 1.0, the bubble effect produced by the micromotor will be

This journal is © The Royal Society of Chemistry 2023

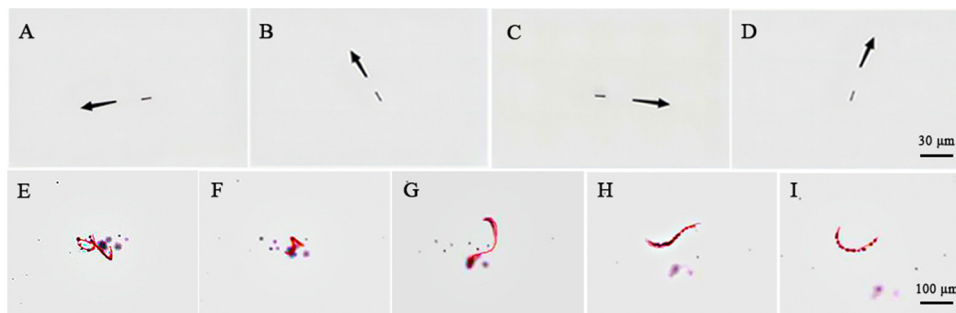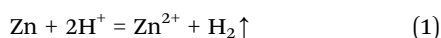*J. Mater. Chem. B*, 2023, **11**, 10728–10737 | **10733**

Fig. 4 Magnetic guidance and kinematic performance images of micromotors: (A)–(D) magnetic guided steering of micromotors. The direction of the red arrow indicates the direction of the magnetic field. (E)–(I) Delay image of the motion path of the micromotor after stable bubbles are generated in the acid solution, with a time interval of 500 ms and pH $\approx$ 1.

different when the HCl solution contains different concentrations of surfactant, as shown in Fig. S5 (ESI†). In scenarios where no surfactant was added in the solution, bubble production from the micromotor is notably minimal. The reason is that the pore size of the micromotor is extremely small, which measures in the nanometer scale. Combined with the substantial surface tension of the solution, swift and smooth access into the micromotor's interior is hindered, thereby limiting its interaction and subsequent reaction with Zn. When the solution contains 1% Triton X-100, the number of bubbles produced is slightly improved, but not highly significant. When the solution contains 2% Triton X-100, the bubbles are considerably more stable. When the solution contains 3% Triton X-100, the number of bubbles is reduced. Thus, when the surfactant content reaches a certain quantity value, the bubble effect produced by the micromotor is at the best state, and as the surfactant content continues to increase, the number of bubbles no longer improves. At this time, the number of bubbles mainly depends on the size of the micromotor aperture and the amount of HCl. Therefore, 2% Triton is more appropriate to use as a surfactant to promote the reaction in the practical application of micromotors.

3.5.2 Motion speed and motion lifetime of micromotors. Given that the innermost layer of the micromotors is metal Zn, Zn reacts to produce gas bubbles in an acidic environment. The reaction formula can be expressed as follows:

$$Zn + 2H^+ = Zn^{2+} + H_2\uparrow \qquad (1)$$

To guarantee uninhibited bubble generation, a cover glass was not utilized on the slide. Thus, the solution on the slide was raised, which produced a stratification effect under the microscope. Different targets may float during bubble generation, making it blurred or even disappear under the field of view. The focal length should be adjusted for clear and precise tracking observation.

A 2 μL of 0.64 mol L^{-1} HCl (containing 2% Triton-X100) and 2 μL of micromotor solution were dropped on the slide and mixed. The pH of the mixed solution was about 1.0. Under the microscope at 20× objective, when the micromotor was immersed in the acid solution, the reaction is initially slow and then becomes fast until it stops. When the acid solution is only in contact with the micromotor, the contact area is small and the reaction is slow, which shows that bubbles are formed slowly at the end of the micromotor, and no movement occurs basically. When the acid solution enters the tube, the bubble generation rate is significantly accelerated, and the movement speed of the micromotor is also significantly improved. As the reaction proceeds, the micromotor shows a random curve motion, as shown in Fig. 4(E)–(I). The motor motion was analyzed, and its speed is directly related to the bubble generation rate, which depends on the solution pH and the contact area of the acid solution with the Zn layer. The movement life is mainly related to the thickness of Zn deposited in the inner layer and the pH of the acid solution. For example, as shown in the motion video of the micromotor in Video S3 (ESI†), the movement speed of the Zn-based micromotor with a length of 5 μm is about 100 μm s^{-1}, and the life span is about 11 s. For the problem that the movement time of the acid-driven imprinted micromotor needs to be prolonged, it can be achieved by increasing the pore size of the polycarbonate film and increasing the amount of Zn deposition in the inner layer.

3.5.3 Prediction of motion speed of micromotors. The movement speed of a micromotor was calculated using a step–strain theoretical model. Referring to the prediction formula for the motion speed of the micromotor in H$_2$O$_2$[31] and improving it to obtain the speed calculation formula for the micromotor in acidic environments follows:

$$v_m = f \times l = \frac{9nm_{Zn}R_mL}{3R_b^2 + LR_b \bigg/ \left(\ln\left(\frac{2L}{R_m}\right) - 0.72 \right)} \qquad (2)$$

where f is the frequency of hydrogen gas bubble generation, l is the step length that each bubble propels the micromotor forward, n is the experimentally measured hydrogen gas generation rate constant, m_{Zn} is the unit mass of Zn, L is the length of the imprinted micromotor, R_m is the inner hole radius of the micromotor, and R_b is the average radius of the bubbles.

According to formula (2), the average speed of micromotor movement is directly proportional to the unit mass of Zn (m_{Zn}), and is related to the length L of the micromotor, the bubble radius R_b, and the inner hole radius of the micromotor R_m. This formula indicates that multiple factors influence the movement

10734 | *J. Mater. Chem. B*, 2023, **11**, 10728–10737

This journal is © The Royal Society of Chemistry 2023

of the micromotor, and its final speed is closely related not only to experimentally related parameters but also to the geometric dimensions of the micromotor's structure and the environmental conditions during movement.

Furthermore, under the condition of a fixed mass of Zn, with n being the experimentally measured hydrogen gas generation rate constant, it was measured as 8.6×10^{-4} m s^{-1}, where the length of the micromotor (L) is 10 μm, and the inner radius of the tube (R_m) is 0.7 μm. When the mass of Zn is lower than a certain value, the radius of the generated bubbles (R_b) should be greater than the inner radius of the micromotor. The diameters are in good agreement with the relationship $R_b = 1.2 R_m$. Therefore, formula (2) can also be simplified as follows:

$$v_m = 9.12 \times 10^{-3} m_{Zn} \tag{3}$$

According to formula (3), with other conditions unchanged, the mass of Zn and the speed of catalyzing the micromotor show a linear relationship. Further experimental results indicate that the maximum calculated movement speed of the micromotor is 100 μm s^{-1}. The relevant experimental calculation results are in good agreement with the experimentally measured results, confirming the validity of this formula. Therefore, the movement speed of the micromotor can be fitted, predicted, and adjusted using the step–strain model.

3.6 Selective capture of phycocyanin by imprinted micromotors

On the basis of the above experimental verification, the acid-driven magnetic imprinting micromotor is successfully synthesized. To further verify the imprinting layer on the surface of the micromotor, 0.5 mg mL^{-1} of phycocyanin solution was added to the imprinting micromotor solution and the non-imprinting micromotor solution for 20 min. The reaction was observed under a laser confocal microscope. Given that the emission wavelength of phycocyanin was usually between 620 nm and 650 nm, the emission wavelength of 633 nm was selected. The red fluorescence can be seen clearly from Fig. 5(A), but the fluorescence image in Fig. S6(A) and (B) (ESI†) showed no observed fluorescence before co-incubation with phycocyanin solution, however, fluorescence was observed after 20 min incubation with 0.5 mg mL^{-1} phycocyanin solution in Fig. S6C (ESI†), which showed that the template proteins on the imprinted micro motors were removed before the co-incubation and successfully adsorbed phycocyanin after the incubation, indicating that the prepared micromotor can recognize and bind phycocyanin in water, and the water was then monitored. However, no red fluorescence corresponds to the micromotors in Fig. 5(B), which represents that the imprinted micromotors have successfully deposited the imprinted layer on the surface of the imprinted micromotors. In comparison with the NIPs, the micromotors imprinted with phycocyanin have better recognition and binding ability to phycocyanin, which is conducive to the adsorption of more phycocyanin, with high sensitivity and easy observation.

Some NIPs also produce red fluorescence. The main reason is that PEDOT/PSS is a substance that is easy to bind to
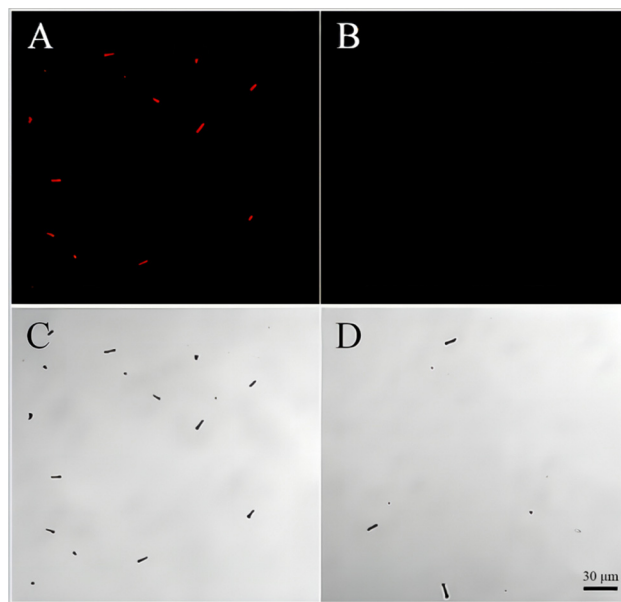

Fig. 5 Laser confocal microscope images of micromotors after adsorbing phycocyanin: (A), (C) imprinted micromotors; (B), (D) NIPs.

proteins, and various interaction forces can be produced between PEDOT/PSS and proteins. In this manner, the protein can firmly bind to the outer layer of the micromotor PEDOT/PSS. PEDOT/PSS was also deposited on the NIP surface, so the NIPs may also have phycocyanin adsorbed on the surface and emit fluorescence. However, the selective adsorption and capture sensitivity of the imprinted micromotors for phycocyanin is still considerably better than that of the NIPs, which can adsorb more target proteins in a shorter time and at a lower concentration.

In the imprinted layer selectivity demonstration experiment, the measured data were analyzed to obtain the ratios of the four proteins after adsorption, as shown in Fig. 6. The concentration of phycocyanin solution after adsorption is 0.2229 mg mL^{-1}, the amount adsorbed is 77.08 μg, the concentration of the BSA solution is 0.2949 mg mL^{-1}, the amount adsorbed is 5.01 μg, the concentration of casein solution is 0.2853 mg mL^{-1}, the amount adsorbed is 7.367 μg, the concentration of β-lactoglobulin solution is 0.2958 mg mL^{-1}, and the amount adsorbed is 4.25 μg. Therefore, the recognition and adsorption of micromotors imprinted with phycocyanin is considerably higher than that of other proteins, which also proves that the imprinted layer is selective. Therefore, the combination of imprinting technology and micromotor actuation is feasible for the selective trapping of substances and load transport.

3.7 Application of phycocyanin-loaded micromotors in cellular environment

Micromotors attached to phycocyanin (single channel), DAPI-stained human hepatocytes (single channel), and a mixture of the two (double channel) were observed by laser confocal microscopy, as shown in Fig. 7. Human hepatocytes show blue fluorescence due to the reaction of the internal DNA with DAPI

This journal is © The Royal Society of Chemistry 2023

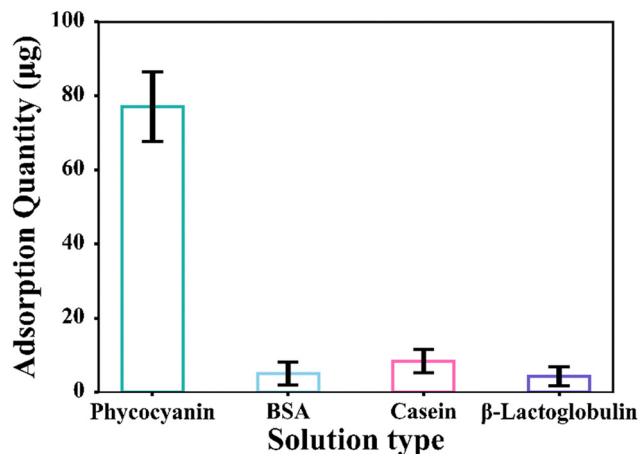*J. Mater. Chem. B*, 2023, **11**, 10728–10737 | **10735**

Fig. 6 Selective adsorption experiments with imprinted micromotors.

staining, and the shape is round. The micromotors show red fluorescence due to the adsorption of phycocyanin and has a long rod-like shape. The fluorescence of micromotors adsorbed with phycocyanin and stained cells can be successfully observed by mixing them together. Besides, we stored the micromotor in deionized water solution for two weeks, and then no Pt and Au were detected in the supernatant, indicating that this micromotor will not produce heavy metal leakage pollution during storage and use.

Subsequently, in order to evaluate the potential toxicity of imprinted micromotor, we used the CCK-8 method to study the cytotoxicity of imprinted micromotors. As shown in Fig. S7 (ESI†), the survival rate of imprinted micromotors on human liver cells increased from 85.66% of the original concentration to 99.25% at 1000 times dilution, indicating that the external imprinting layer of the micromotor had relatively low cytotoxicity to cells and the toxicity of internal heavy metal ions was within a controllable range, it will not cause serious damage to the organism when acting inside the human body.

Thus, the micromotors can also be applied to complex cellular environments, in addition to the current widely used water environment, which is conducive to expanding the application scenarios and fields of micromotors and laying a certain foundation for *in vivo* drug delivery in the future.

4. Conclusion

In this study, on the basis of selective binding of PEDOT/PSS to proteins, acid-driven magnetic imprinting micromotors were successfully prepared by combining MIP with self-driven micromotors by template electrodeposition method. The micromotor has a tubular shape and strong magnetism, which can perform accurate magnetic guidance steering. In a strongly acidic environment, when the content of Triton X-100 is 2%, a large number of stable bubbles are generated, which drives the micromotor to move. In view of the strong fluorescence of phycocyanin, under the laser confocal microscope, the micromotor imprinted with phycocyanin can recognize and adsorb phycocyanin. The result demonstrates the high selectivity of imprinted micromotors, and the adsorption results can be easily observed. This result proves the feasibility and broad prospect of the combination of imprinting technology and micromotor driving technology in selective material loading and precise transport. In addition, the prepared micromotor contains metal Zn, which is one of the essential trace elements for the human body, and cytotoxicity experiments have shown that acid driven imprinted micromotors have no cytotoxicity. It is expected to be applied to the human stomach environment in the future.
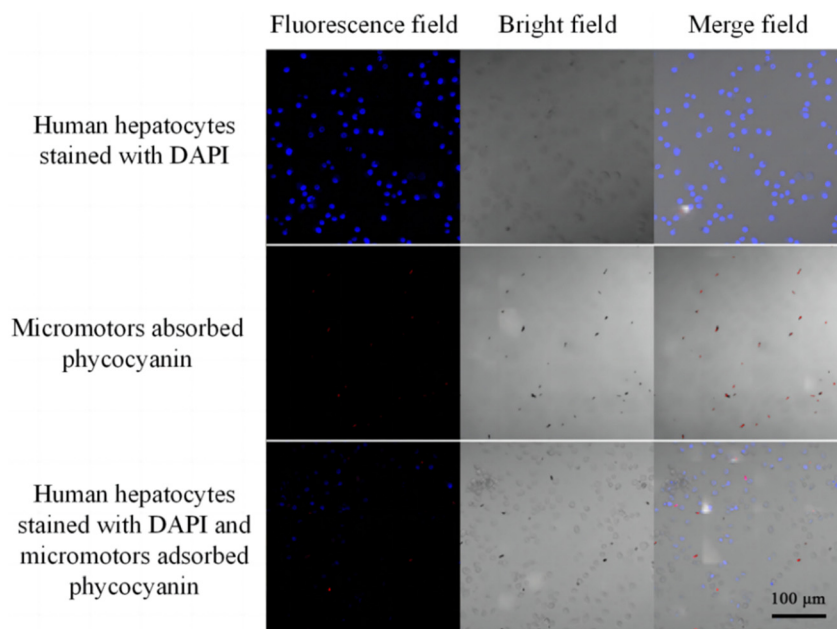

Fig. 7 Laser confocal microscope images of micromotors in the cellular environment.

Author contributions

Guangdong Yang: methodology, data curation, writing original draft and editing. Jiajing Liu: data curation, writing original draft and editing. Zhong Zhang: conceptualization, writing reviewing, project administration, funding acquisition. Hongye Tian: writing reviewing. Li Yuan, writing reviewing. Xingbin Yang: project administration, funding acquisition.

Conflicts of interest

There are no conflicts to declare.

Acknowledgements

References

1 W. Yang, J. Li, Z. Xu, J. Yang, Y. Liu and L. Liu, *J. Mater. Chem. C*, 2019, **7**, 10297–10308.

2 M. Zhou, T. Hou, J. Li, S. Yu, Z. Xu, M. Yin, J. Wang and X. Wang, *ACS Nano*, 2019, **13**, 1324–1332.

3 Y. Yang, K. Hu, P. Zhang, P. Zhou, X. Duan, H. Sun and S. Wang, *Small*, 2021, **17**, 2100927.

4 D. Kagan, S. Campuzano, S. Balasubramanian, F. Kuralay, G.-U. Flechsig and J. Wang, *Nano Lett.*, 2011, **11**, 2083–2087.

5 Q. Wang, R. Dong, Q. Yang, J. Wang, S. Xu and Y. Cai, *Nanoscale Horiz.*, 2020, **5**, 325–330.

6 V. de la Asunción-Nadal, D. Rojas, B. Jurado-Sánchez and A. Escarpa, *J. Mater. Chem. A*, 2023, **11**, 1239–1245.

7 C. C. Mayorga-Martinez, J. Vyskočil, F. Novotný and M. Pumera, *J. Mater. Chem. A*, 2021, **9**, 14904–14910.

8 G. Loget and A. Kuhn, *Nat. Commun.*, 2011, **2**, 535.

9 D. Zhang, D. Wang, J. Li, X. Xu, H. Zhang, R. Duan, B. Song, D. Zhang and B. Dong, *J. Mater. Sci.*, 2019, **54**, 7322–7332.

10 X. Bing, X. Zhang, J. Li, D. H. L. Ng, W. Yang and J. Yang, *J. Mater. Chem. A*, 2020, **8**, 2809–2819.

11 W. Gao, X. Feng, A. Pei, Y. Gu, J. Li and J. Wang, *Nanoscale*, 2013, **5**, 4696–4700.

12 X. Chang, C. Chen, J. Li, X. Lu, Y. Liang, D. Zhou, H. Wang, G. Zhang, T. Li, J. Wang and L. Li, *ACS Appl. Mater. Interfaces*, 2019, **11**, 28507–28514.

13 W. Gao, A. Pei, R. Dong and J. Wang, *J. Am. Chem. Soc.*, 2014, **136**, 2276–2279.

14 W. Gao, A. Uygun and J. Wang, *J. Am. Chem. Soc.*, 2011, **134**, 897–900.

15 R. F. Ismagilov, A. Schwartz, N. Bowden and G. M. Whitesides, *Angew. Chem., Int. Ed.*, 2002, **41**, 652–654.

16 W. F. Paxton, K. C. Kistler, C. C. Olmeda, A. Sen, S. K. St. Angelo, Y. Cao, T. E. Mallouk, P. E. Lammert and V. H. Crespi, *J. Am. Chem. Soc.*, 2004, **126**, 13424–13431.

17 J. Li, S. Sattayasamitsathit, R. Dong, W. Gao, R. Tam, X. Feng, S. Ai and J. Wang, *Nanoscale*, 2014, **6**, 9415–9420.

18 S. Giudicatti, S. M. Marz, L. Soler, A. Madani, M. R. Jorgensen, S. Sanchez and O. G. Schmidt, *J. Mater. Chem. C*, 2014, **2**, 5892–5901.

19 A. Zenerino, C. Peyratout and A. Aimable, *J. Colloid Interface Sci.*, 2015, **450**, 174–181.

20 C. E. Sing, L. Schmid, M. F. Schneider, T. Franke and A. Alexander-Katz, *Proc. Natl. Acad. Sci. U. S. A.*, 2009, **107**, 535–540.

21 W. Wang, S. Li, L. Mair, S. Ahmed, T. J. Huang and T. E. Mallouk, *Angew. Chem., Int. Ed.*, 2014, **53**, 3201–3204.

22 O. E. Shklyaev, H. Shum, V. V. Yashin and A. C. Balazs, *Langmuir*, 2017, **33**, 7873–7880.

23 L. Chen, X. Wang, W. Lu, X. Wu and J. Li, *Chem. Soc. Rev.*, 2016, **45**, 2137–2211.

24 J. Orozco, A. Cortés, G. Cheng, S. Sattayasamitsathit, W. Gao, X. Feng, Y. Shen and J. Wang, *J. Am. Chem. Soc.*, 2013, **135**, 5336–5339.

25 N. T. Eriksen, *Appl. Microbiol. Biotechnol.*, 2008, **80**, 1–14.

26 Z. Zhang, L. Chen, F. Yang and J. Li, *RSC Adv.*, 2014, **4**, 31507–31514.

27 D. Hu, Z. Zhang, L. Yuan, W. Li, Y. Guo, R. Zhang, X. Yang and H. Peng, *Int. J. Biol. Macromol.*, 2021, **193**, 127–136.

28 Z. Zhang, J. Li, L. Fu, D. Liu and L. Chen, *J. Mater. Chem. A*, 2015, **3**, 7437–7444.

29 A. Menaker, V. Syritski, J. Reut, A. Öpik, V. Horváth and R. E. Gyurcsányi, *Adv. Mater.*, 2009, **21**, 2271–2275.

30 G. Lautner, J. Kaev, J. Reut, A. Öpik, J. Rappich, V. Syritski and R. E. Gyurcsányi, *Adv. Funct. Mater.*, 2010, **21**, 591–597.

31 M. García, J. Orozco, M. Guix, W. Gao, S. Sattayasamitsathit, A. Escarpa, A. Merkoçi and J. Wang, *Nanoscale*, 2013, **5**, 1325–1331.

This journal is © The Royal Society of Chemistry 2023

J. Mater. Chem. B, 2023, **11**, 10728–10737 | **10737**